Nanosized BiOX (X = Cl, Br, I) Particles Synthesized in Reverse Microemulsions

J. Henle,[‡] P. Simon,[§] A. Frenzel,[‡] S. Scholz,[‡] and S. Kaskel*[,†]

Department of Inorganic Chemistry, Technical University of Dresden, Mommsenstrasse 6, 01069 Dresden, Germany; Department of Inorganic Chemistry, Technical University of Dresden, Mommsenstrasse 6, 01069 Dresden, Germany; and Max Planck Institute for Chemical Physics of Solids, Nöthnitzer Strasse 40, 01187 Dresden, Germany

Received July 18, 2006. Revised Manuscript Received October 30, 2006

Reverse microemulsions, consisting of heptane, nonionic surfactants, and aqueous salt solutions, were used to synthesize BiOX (X = Cl, Br, I) nanoparticles. The reverse micelles act as nanoscale templates for the ionic precipitation process. The size of the micelles can be used to tailor the size of the particles. BiOCl nanoparticles were synthesized in a range of 3−22 nm (diameter); for BiOBr and BiOI, the range was 5.5−22 nm and 4−18 nm, respectively. The reverse microemulsions were characterized by dynamic light scattering. X-ray diffraction patterns of the particles isolated from the microemulsions clearly demonstrate the influence of the water/surfactant ratio (R_w) of the microemulsions on the crystallite size. Also, the concentration of the involved salt solutions affects the particle diameter. For BiOI nanoparticles, a significant dependence of the band gap energy on the particle diameter was observed using UV−vis spectroscopy. Depending on the size of the particles, the color varied from pale yellow to dark orange. Atomic force microscopy of BiOI nanoparticles on a mica substrate revealed well-separated particles with a narrow size distribution.

Introduction

The preparation of nanoparticles has become a very active research area in recent years.[1] Nanosized materials have applications in catalysis, electronics, miniaturization, and ceramics; physical properties attributed to the reduction of dimensions, like the quantum-size effect, are of fundamental interest. In particular, control over particle shape, size, and size distribution is a key target. Since the complex process of nucleation and nanocrystal growth is difficult to control, precipitation reactions often lead to broad particle size distributions. To overcome these problems, reverse microemulsions are used as a reaction medium for the preparation of nanoparticles. Reverse microemulsions consist of aqueous droplets 2−20 nm in diameter, encapsulated by surfactant molecules and surrounded by an oil phase. They were used as templates in material syntheses by Boutonnet et al. already in 1982,[2] and since then, the method has gained importance more and more in the last few decades. The fundamentals of nanoparticle syntheses in microemulsions have been described by Lade et al.[3] and in several monographs.[4−6] Different materials have been synthesized in reverse micelles, and applications are widespread. Different kinds of catalysts,[7−9] oxides, and ceramic materials such as $Ba(Mg_{1/3}Ta_{2/3})O_3$,[10] $BaAl_{12}O_{19}$,[11] aluminum oxide-hydroxide,[12] ZnO,[13,14] ZrO_2,[15] cerium oxide,[16,17] TiO_2,[18,19] iron oxide,[20,21] and $BaTiO_3$[22,23] were prepared. Recent investigations also focused on materials with exotic morphologies, such as V_2O_5—[24] or Sb_2O_3/Sb_2O_5 nanorods.[25] Also, several composites have been

* To whom correspondence should be addressed. Phone: 49-351-46333632. Fax: 49-351-46337287. E-mail: Stefan.Kaskel@chemie.tu-dresden.de.
† Department of Inorganic Chemistry, Technical University of Dresden.
‡ Department of Inorganic Chemistry, Technical University of Dresden.
§ Max Planck Institute for Chemical Physics of Solids.

(1) Klabunde, K. J. *Nanoscale Materials in Chemistry*; Wiley VCH: New York, 2001.
(2) Boutonnet, M.; Kizling, J.; Stenius, P. *Colloids Surf.* **1982**, *5*, 209.
(3) Lade, M.; Mays, H.; Schmidt, J.; Willumeit, R.; Schomäcker, R. *Colloids Surf., A* **2000**, *163*, 3.
(4) Kumar, P.; Mittal, K. L. *Handbook of Microemulsion Science and Technology*; Marcel Dekker: New York, 1999.
(5) Texter, J. *Reactions and Synthesis in Surfactant Systems*; Marcel Dekker: New York, 2001.
(6) Uskokovic, V.; Drofenik, M. *Surf. Rev. Lett.* **2005**, *12*, 239.
(7) Dadyburjor, D. B.; Fout, T. E.; Zondlo, J. W. *Catal. Today* **2000**, *63*, 33.
(8) de Jesus, D. M.; Spiro, M. *Langmuir* **2000**, *16*, 4896.
(9) Hayashi, H.; Murata, S.; Tago, T.; Kishida, M.; Wakabayashi, K. *Chem. Lett.* **2001**, 34.
(10) Lee, Y. C.; Liang, M. H.; Hu, C. T.; Lin, I. N. *J. Eur. Ceram. Soc.* **2001**, *21*, 2755.
(11) Zarur, A. J.; Ying, J. Y. *Nature* **2000**, *403*, 65.
(12) Berkovich, Y.; Aserin, A.; Wachtel, E.; Garti, N. *J. Colloid Interface Sci.* **2002**, *245*, 58.
(13) Hingorani, S.; Pillai, V.; Kumar, P.; Multani, M. S.; Shah, D. O. *Mater. Res. Bull.* **1993**, *28*, 1303.
(14) Lim, B. P.; Wang, J.; Ng, S. C.; Chew, C. H.; Gan, L. M. *Ceram. Int.* **1998**, *24*, 205.
(15) Althues, H.; Kaskel, S. *Langmuir* **2002**, *18*, 7428.
(16) Masui, T.; Fujiwara, K.; Machida, K.; Adachi, G.; Sakata, T.; Mori, H. *Chem. Mater.* **1997**, *9*, 2197.
(17) Zhang, J.; Ju, X.; Wu, Z. Y.; Liu, T.; Hu, T. D.; Xie, Y. N.; Zhang, Z. L. *Chem. Mater.* **2001**, *13*, 4192.
(18) Kim, E. J.; Hahn, S. H. *Mater. Lett.* **2001**, *49*, 244.
(19) Boutonnet, M.; Kizling, J.; Bigey, C.; Touroude, R. *Appl. Catal., A* **1996**, *135*, L13.
(20) Lopez Perez, J. A.; Lopez Quintela, M. A.; Mira, J.; Rivas, J.; Charles, S. W. *J. Phys. Chem. B* **1997**, *101*, 8045.
(21) Dresco, P. A.; Zaitsev, V. S.; Gambino, R. J.; Chu, B. *Langmuir* **1999**, *15*, 1945.
(22) Herrig, H.; Hempelmann, R. *Nanostruct. Mater.* **1997**, *9*, 241.
(23) Beck, C.; Härtl, W.; Hempelmann, R. *J. Mater. Res.* **1998**, *13*, 3174.
(24) Pinna, N.; Willinger, M.; Weiss, K.; Urban, J.; Schlogl, R. *Nano Lett.* **2003**, *3*, 1131.
(25) Guo, L.; Wu, Z. H.; Liu, T.; Wang, W. D.; Zhu, H. S. *Chem. Phys. Lett.* **2000**, *318*, 49.

10.1021/cm061671k CCC: $37.00
Published on Web 01/12/2007

Scheme 1. Two-Microemulsion Approach as Applied for the Synthesis of BiOX Nanoparticles

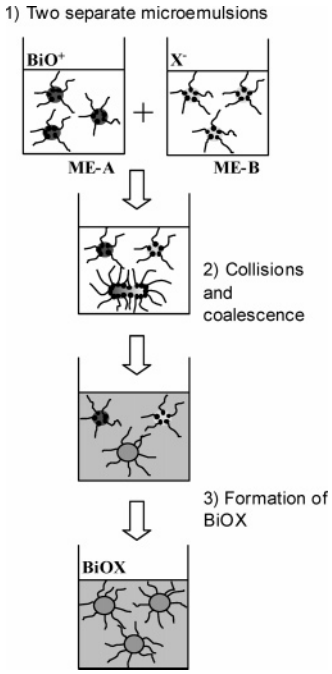

prepared, such as silica-coated cobalt particles,[26] or Pd/SiO_2.[27]

Particle formation in reverse micelles can be achieved in different ways. In the single-microemulsion approach, one microemulsion is prepared and, subsequently, a precursor or reactant is added, diffusing through the oil phase to the micelles containing a reactant. This method is frequently used in space-confined sol−gel processes for the synthesis of oxide nanoparticles by hydrolysis and condensation of alkoxide precursors within the nanosized water droplets.[15,28,29] Other procedures use the possibility to integrate one of the reactants as the counterion of ionic surfactant molecules.[30] A second processing route, a multi-microemulsion route, takes advantage of two or more separately prepared microemulsions of the same water/surfactant/oil ratio, but with each microemulsion containing one of the necessary reactants for the particle synthesis (Scheme 1). After mixing the microemulsions together, the particle formation occurs by intermicellar exchange of the reactants. Comparative studies have shown that the multi-microemulsion route yields finer particles and narrow size distributions.[31,32]

Regarding the aqueous micelles as nanoreactors for particle synthesis, a direct connection between size and shape of the micelles and that of the obtained particles can be assumed, even though particle and micelle diameter do not need to be identical. In several cases, control of nanoparticle size with the water droplet size was demonstrated.[33,34] Therefore, substantial interest lies in the determination of the structural properties such as sizes and shapes of micelles and their dynamics. Great effort is put in attempts to model reverse micellar structures,[35,36] but also in experimental methods, such as conductivity measurements[37] and spectroscopic[38,39] and scattering[40] methods.

There are many factors that have an influence on the properties of micelles and of the produced particles. The parameter that is supposed to be the most decisive parameter affecting the size of reverse micelles is the water-to-surfactant molar ratio (R_w). For AOT-based microemulsions, a linear relation could be found between this ratio and the size of the reverse micelles.[34,41] The same experimental results indicate that temperature, organic solvent, type and concentration of the surfactant, and electrolytes also play a significant role. A direct connection between water content and size of synthesized particles was confirmed for many systems.[33,34,42] However, for several examples, this relationship was reversed or no relationship could be found at all.[21,43] These examples demonstrate that the model of water droplets as nanotemplates for particle synthesis can be assumed only if the structure of the micelles is maintained during the reaction.

In the following, we will present the application of a multi-microemulsion route for the synthesis of BiOX (X = Cl, Br, I) nanoparticles. Bismuth oxyhalides, especially BiOCl, have industrial applications as pigments in the cosmetic industry.[44−48] BiOCl is also known as a catalyst, e.g., for oxidative cracking of *n*-butane.[49] Controlled synthesis of BiOX nanoparticles is crucial for the better dispersibility of pigments and enhancement of catalytic performance. The optical properties of nanosized color pigments of BiOI are promising for the preparation of new transparent nanocomposite materials. Bismuth oxyhalides are V−VI−VII group compound semiconductors with tetragonal crystal structure. The nanocrystals can be synthesized with sufficient crystal-

(26) Wu, M. Z.; Zhang, Y. D.; Hui, S.; Xiao, T. D.; Ge, S. H.; Hines, W. A.; Budnick, J. I. *J. Appl. Phys.* **2002**, *92*, 491.
(27) Bae, D. S.; Han, K. S.; Adair, J. H. *J. Mater. Chem.* **2002**, *12*, 3117.
(28) Palkovits, R.; Althues, H.; Rumplecker, A.; Tesche, B.; Dreier, A.; Holle, U.; Fink, G.; Cheng, C. H.; Shantz, D. F.; Kaskel, S. *Langmuir* **2005**, *21*, 6048.
(29) Grasset, F.; Labhsetwar, N.; Li, D.; Park, D. C.; Saito, N.; Haneda, H.; Cador, O.; Roisnel, T.; Mornet, S.; Duguet, E.; Portier, J.; Etourneau, J. *Langmuir* **2002**, *18*, 8209.
(30) Pileni, M. P.; Motte, L.; Petit, C. *Chem. Mater.* **1992**, *4*, 338.
(31) Wang, J. A.; Valenzuela, M. A.; Salmones, J.; Vazquez, A.; Garcia-Ruiz, A.; Bokhimi, X. *Catal. Today* **2001**, *68*, 21.
(32) Fang, J. Y.; Wang, J.; Ng, S. C.; Chew, C. H.; Gan, L. M. *Nanostruct. Mater.* **1997**, *8*, 499.
(33) Carpenter, E. E.; Seip, C. T.; O'Connor, C. J. *J. Appl. Phys.* **1999**, *85*, 5184.
(34) Pileni, M. P.; Zemb, T.; Petit, C. *Chem. Phys. Lett.* **1985**, *118*, 414.
(35) Levinger, N. E. *Science* **2002**, *298*, 1722.
(36) Senapati, S.; Berkowitz, M. L. *J. Chem. Phys.* **2003**, *118*, 1937.
(37) Benito, I.; Garcia, M. A.; Monge, C.; Saz, J. M.; Marina, M. L. *Colloids Surf.* **1997**, *125*, 221.
(38) Patzlaff, T.; Janich, M.; Seifert, G.; Graener, H. *Chem. Phys.* **2000**, *261*, 381.
(39) Zhong, Q.; Steinhurst, D. A.; Carpenter, E. E.; Owrutsky, J. C. *Langmuir* **2002**, *18*, 7401.
(40) Brunetti, S.; Roux, D.; Bellocq, A. M.; Fourche, G.; Bothorel, P. *J. Phys. Chem.* **1983**, *87*, 1028.
(41) Pileni, M. P. *J. Phys. Chem.* **1993**, *97*, 6961.
(42) Steytler, D. C.; Gurgel, A.; Ohly, R.; Jung, M.; Heenan, R. K. *Langmuir* **2004**, *20*, 3509.
(43) Barnickel, P.; Wokaun, A.; Sager, W.; Eicke, H. F. *J. Colloid Interface Sci.* **1992**, *148*, 80.
(44) Heider, L.; Loch, M.; Schupp, N.; Kniess, H. B. German Patent Application, DE20011051844 20011024, 2002.
(45) Buxbaum, G.; Pfaff, G. *Industrial Inorganic Pigments*; Wiley-VCH: Weinheim, Germany, 2005.
(46) Draelos, Z. D. *Clin. Dermatol.* **2001**, *19*, 424.
(47) Maile, F. J.; Pfaff, G.; Reynders, P. *Prog. Org. Coat.* **2005**, *54*, 150.
(48) Pfaff, G.; Reynders, P. *Chem. Rev.* **1999**, *99*, 1963.
(49) Kijima, N.; Matano, K.; Saito, M.; Oikawa, T.; Konishi, T.; Yasuda, H.; Sato, T.; Yoshimura, Y. *Appl. Catal., A* **2001**, *206*, 237.

Table 1. Compositions of the Microemulsions Me-2−Me-10 Used

name	R_w	H_2O (wt %)	heptane (wt %)	NP5 (wt %)	viscosity[a] (cP)
ME2	2	4.5	40.8	54.7	13.01
ME4	4	6.1	55.8	38.1	7.86
ME6	6	7	64	29	3.99
ME8	8	7.6	69.2	23.2	3.14
ME10	10	8	73	19	2.74

[a] Measured for ME containing 0.1 mol/L $Bi(NO_3)_3$ in the aqueous phase.

Table 2. Compositions of Diluted Microemulsions Me-2−Me-10 for DLS Measurements

name	R_w	H_2O (wt %)	heptane (wt %)	NP5 (wt %)	viscosity[a] (cP)	micelle size[a] (z-av./nm)
ME2-d	2	1.6	79	19.4	0.85	4.9
ME4-d	4	1.7	87.4	10.9	0.63	7.0
ME6-d	6	1.8	90.7	7.5	0.58	10.3
ME8-d	8	1.8	92.5	5.7	0.56	16.0
ME10-d	10	1.9	93.7	4.5	0.47	25.5

[a] Measured for ME containing 0.1mol/L $Bi(NO_3)_3$ in the aqueous phase.

linity at room temperature without the necessity of subsequent thermal treatments. By systematic variation of the synthesis conditions, especially the composition of the microemulsions and the concentration of the involved salt solutions, we will discuss the crucial parameters affecting the size of the prepared nanocrystals.

Experimental Section

Microemulsion. Marlophen NP5 ($RO(CH_2CH_2O)_xH$, $x = 5$, R = nonylphenyl, $M = 440$ g/mol, SASOL) was chosen as the surfactant. The phase diagram was obtained by adding the surfactant to mixtures of *n*-heptane (>99%, Aldrich) and deionized water under vigorous stirring at 20 °C until the microemulsions appear transparent. The equilibration time was 15 min. The reverse microemulsions were set aside to verify that phase separation would not occur after stirring was stopped. All microemulsions remained stable for at least 24 h.

Syntheses. Microemulsions were prepared as explained above. The aqueous phase of the microemulsions contained salt solutions of $Bi(NO_3)_3 \cdot 5H_2O$ (99.99%, Aldrich) (in the following identified as ME-A) or NaCl, KBr, or KI as counterions (ME-B). $Bi(NO_3)_3$ was dissolved as BiO^+ in water by adding stoichiometric amounts of mannitol and levigating both with 1−2 drops of water. Tables 1 and 2 give the compositions of the microemulsions used and the concentrations of the salt solutions in the aqueous phases. In a two-microemulsion approach, two separate microemulsions of the same contents of oil, water, and surfactant were prepared for each reactant involved. One microemulsion containing BiO^+ was added to a corresponding microemulsion containing the counterion. The mixed microemulsion was stirred for 24 h, and the white or colored precipitate was isolated by centrifugation and washed with heptane and ethanol. Some microemulsions did not show any turbidity after 24 h. To isolate particles from these microemulsions, heptane was removed with a rotating evaporator until the particles precipitated.

Viscosimetry. The viscosity of all microemulsions was measured at 20 °C with Ubbelohde viscosimeters Type 532-01-0a and Type 532-13-Ic by Schott. The mean value out of four measurements is given.

Dynamic Light Scattering (DLS). The reverse microemulsions were characterized by DLS using a Zetasizer Nano ZS from Malvern Instruments. The micelle sizes of ME-A and ME-B as well as the particle size after the reaction were measured at 20 °C. For DLS measurements, the measured viscosities of the microemulsions were used. Average particle diameters (*z*-average) were determined from intensity weighed size distributions, calculated using the NNLS-algorithm.

UV−Vis Spectroscopy. UV−vis spectra of the microemulsions containing BiOI nanoparticles were measured on a Shimadzu UV−vis spectrophotometer UV-1650PC. The spectra were recorded 30 min after mixing the two microemulsions containing $Bi(NO_3)_3$ and KI. The absorbance was measured using 1 mm thick cuvettes. As reference samples, microemulsions without BiOI particles containing the same amount of surfactant were chosen. The absorption onset was determined as the intersection of the steep absorption and the background via linear regression.

X-ray Diffraction (XRD). XRD powder patterns were recorded in transmission geometry using a Stoe Stadi-P diffractometer and Cu $K\alpha_1$ radiation ($\lambda = 0.154\,05$ nm). For crystallite size determinations, the single-line size/strain analysis (WinXPow, Stoe) was used. For correction of the instrumental broadening, a LaB_6 standard sample was used.

Transmission Electron Microscopy (TEM). Samples for TEM analysis were prepared by dipping copper grids into microemulsions containing BiOI particles. Transmission electron micrographs were obtained using a Philips CM200 FEG\ST-Lorentz electron microscope with a field emission gun at an acceleration voltage of 200 kV. The experiments were carried out at the Special Laboratory Triebenberg for Electron Holography and High-Resolution Microscopy of the Technical University Dresden, Germany.

Results and Discussion

A two-microemulsion approach was used for the synthesis of BiOX nanoparticles in reverse micelles. The method can be considered as an ionic precipitation process, taking place in the core of reverse micelles as nanoscale hydrophilic cavities. Three major steps can be identified during the process (Scheme 1). First, two separate microemulsions are prepared: one containing salt solutions of $Bi(NO_3)_3$ as the aqueous phase and one containing the corresponding counterions to precipitate BiOCl, BiOBr, or BiOI (Step 1). Mixing of two microemulsions with equal volumes leads to the formation of the product. Since the reverse micelles move rapidly, the nanodroplets containing the reactants can diffuse through the continuous phase and collide with each other. As a result of these collisions, the droplets coalesce and temporarily merge with each other (Step 2). In these temporarily merged micelles, the surfactant layers are opened partially and dissolved reactants can exchange within the merged droplets. Subsequently, the fused micelles separate again, and average size and number of micelles remain

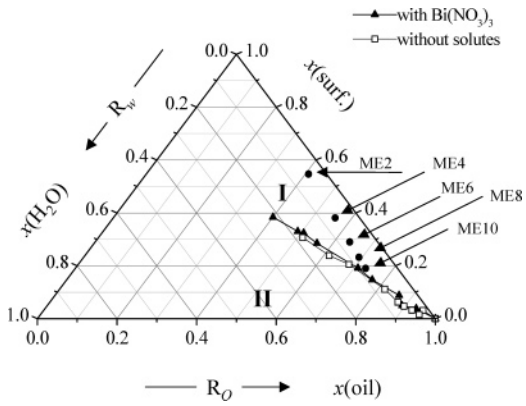

Figure 1. Oil-rich region of the phase diagram for Marlophen NP5/heptane/water with and without solutes in the aqueous phase (I = isotropic solution, II = two-phase region, x = mass fraction). The solid circles mark the used compositions for microemulsions ME2−ME10 with increasing R_w.

constant. In a third step, the BiOX particles are formed within the nanodroplets according to the following equation:

$$Bi(NO_3)_3 + NaX + H_2O \rightarrow BiOX + NaNO_3 + 2HNO_3 \qquad X = Cl, Br, I$$

Reactants and products of the reaction strongly affect the stability of the microemulsion; therefore, it was necessary to find stable compositions for the used microemulsions. In the synthesis of BiOX particles, we succeeded in finding at least one composition for each of the systems, in which the microemulsions remained stable even after formation of the particles and no irreversible coalescence appeared. Even though most of the microemulsions became unstable after particle precipitation, particles separated from the liquid phase of all microemulsions by centrifugation were nanocrystalline.

To locate the one-phase region of the ternary phase diagram, surfactant was added to mixtures of *n*-heptane and aqueous $Bi(NO_3)_3$ solution. The properties of the microemulsions are directly connected to the size and shape of the generated particles. The micelle size depends on the composition of the microemulsion, the surfactant, and the temperature. Marlophen NP5 was chosen as the surfactant because the hydrophilic−lipophilic balance (HLB) is low and the surfactant/heptane mixture is able to solubilize relatively high amounts of water. A small influence of the salt solutions on the phase diagrams was observed. Compared to the corresponding microemulsions without solutes in the aqueous phases, a slight shift of the phase boundary toward higher surfactant content could be observed (Figure 1). Between the different salts $Bi(NO_3)_3$, NaCl, KBr, and KI, no significant change, either for the position of the phase boundary nor for the size of the micelles determined by dynamic light scattering, was observed for the concentrations used. At constant temperature, the most important parameter affecting the micelle size is the molar water/surfactant ratio:

$$R_w = \frac{n(H_2O)}{n(\text{Surfact.})}$$

Typically, with increasing R_w, the water droplets increase as well. Keeping the water concentration constant, the volume of reverse micelles can be decreased by adding surfactant. Since the micelles represent nanoscale exotemplates for particle syntheses, a direct connection to particle size can be expected. Stable isotropic solutions were prepared with R_w-values between 2 and 10. Table 1 shows the compositions of the microemulsions with increasing R_w-value. For the discussion of the microemulsions, the R_w-value is not sufficient. Also, the molar ratio oil/water,

$$R_O = \frac{n(\text{Oil})}{n(H_2O)}$$

is crucial for the stability of the microemulsion. In our experiments, the R_O-value was kept small in order to achieve high yields. Also, in order to obtain microemulsions that remain stable after the formation of BiOX nanoparticles, we decided to use compositions not too close to the phase boundary. For better comparison, the R_O-value was kept constant at 1.6. The compositions of the microemulsions used for the preparation of the particles are marked as solid circles in the phase diagram in Figure 1.

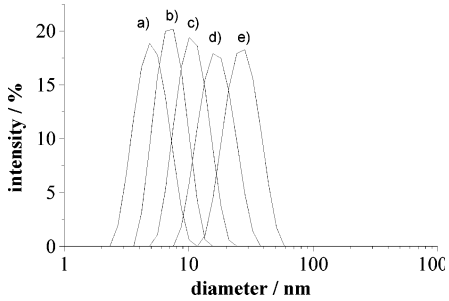

Figure 2. Size distributions (DLS) of micelles in microemulsions ME2-d, ME4-d, ME6-d, ME8-d, and ME10-d with increasing R_w from (a) to (e).

Materials Characterization. (a) Dynamic Light Scattering. The viscosities given in Table 1 indicate interaction of the micelles due to the high concentration. Since the micelle size is calculated using the Stokes Einstein equation, assuming infinite dilution, we used highly diluted microemulsions for DLS measurements in order to get an impression of the relative size of the micelles with increasing R_w.

For dynamic light scattering measurements, microemulsions with increasing R_w from 2 to 10 were prepared. The compositions of the microemulsions used are given in Table 2. The R_O-values were kept constant at 9. The size distribution of micelles was measured at 20 °C. Figure 2 gives size distributions of micelles in microemulsions with increasing R_w-values. The micelle size increases from $R_w = 2$ (5 nm) to $R_w = 10$ (25.5 nm). Microemulsions with different salt solutions in the aqueous phase were measured as well. However, for all microemulsions, the obtained size distributions were almost identical to those of the corresponding salt-free microemulsion, irrespective of the salt solutions, indicating that the influence of the salts, at least for low concentrations, was negligible and the micelle size was controlled only by the water/surfactant/oil ratio of the microemulsions.

Twenty-four hours after mixing the microemulsions containing $Bi(NO_3)_3$ (ME-A) and counterions (ME-B) in the aqueous phases, dynamic light scattering was measured again for the microemulsions containing BiOX particles. Figure 3 gives size distributions for one microemulsion ($R_w = 8$)

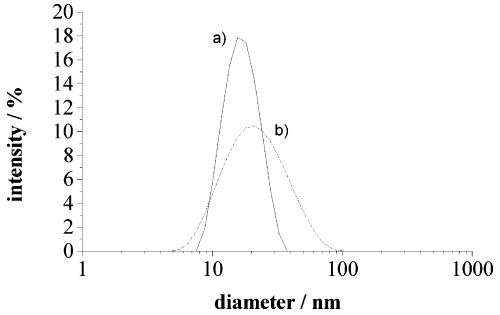

Figure 3. Size distribution (DLS) in microemulsions ($R_w = 8$) (a) before and (b) 24 h after formation of BiOI nanoparticles.

Table 3. Compositions of the Aqueous Phases of All Microemulsions; For All Samples BiOX-1−BiOX-15, Two Microemulsions Me-A and Me-B Were Used

name	R_w	$c(Bi(NO_3)_3)$ (mol/L) in ME-A	c(NaCl) (mol/L) in ME-B	c(KBr) (mol/L) in ME-B	c(KI) (mol/L) in ME-B
BiOX-1	2	0.1	0.1	0.1	0.1
BiOX-2	4	0.1	0.1	0.1	0.1
BiOX-3	6	0.1	0.1	0.1	0.1
BiOX-4	8	0.1	0.1	0.1	0.1
BiOX-5	10	0.1	0.1	0.1	0.1
BiOX-6	2	0.1	0.05	0.05	0.05
BiOX-7	4	0.1	0.05	0.05	0.05
BiOX-8	6	0.1	0.05	0.05	0.05
BiOX-9	8	0.1	0.05	0.05	0.05
BiOX-10	10	0.1	0.05	0.05	0.05
BiOX-11	2	0.05	0.1	0.1	0.1
BiOX-12	4	0.05	0.1	0.1	0.1
BiOX-13	6	0.05	0.1	0.1	0.1
BiOX-14	8	0.05	0.1	0.1	0.1
BiOX-15	10	0.05	0.1	0.1	0.1

containing $Bi(NO_3)_3$ (Figure 3a) and for the mixed microemulsion of ME-A and ME-B containing BiOI particles after 24 h of stirring (Figure 3b). The size distribution for the initial microemulsion ME-A was narrow; the average micelle diameter was 16 nm. The mixed microemulsion (BiOI-4) is stable and transparent after 24 h of stirring, and the average particle diameter is 17.5 nm. The size distribution curve is broader than the curve for ME-A and ME-B. Despite this broader distribution, the particles seem to be monodisperse in this microemulsion (see TEM, Figure 8). Similar results could be obtained for various microemulsions, depending on the synthesized particles, R_w, and salt concentrations. Stable microemulsions with monodisperse particles were obtained for the samples BiOCl-2, BiOCl-7, BiOCl-8, BiOBr-6, BiOI-4, BiOI-5, BiOI-10, BiOI-13, and BiOI-14. The corresponding compositions and salt concentrations of these samples are given in Tables 1 and 3. However, most of the microemulsions showed turbidity after particle formation, and the size distributions in dynamic light scattering indicated strong agglomeration effects.

(b) UV−Vis Spectroscopy. The color of bulk BiOI is described in the literature as carmine red, and the absorption edge is 1.94 eV.[50] In UV−vis spectra, the corresponding absorption band in the visible region is detected at 656 nm. The formation of BiOI in the mixed microemulsions could be followed with the naked eye. Immediately after adding the two transparent microemulsions together, the color changed.

(50) Shtilikh, Mv.; Chepur, D. V. *Sov. Phys. Semicond.* **1972**, *6*, 962.

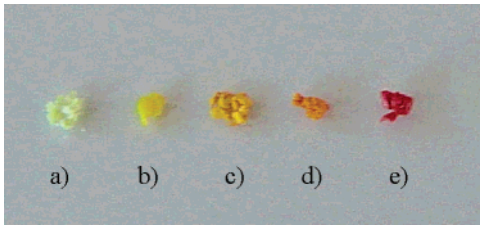

Figure 4. Photograph of BiOI particles separated from microemulsions by centrifugation: (a)−(d) increasing $R_w = 2$, 4, 6, and 8 at stoichiometric salt concentrations, respectively; (e) $R_w = 10$, ratio $BiO^+/I^- = 0.5:1$.

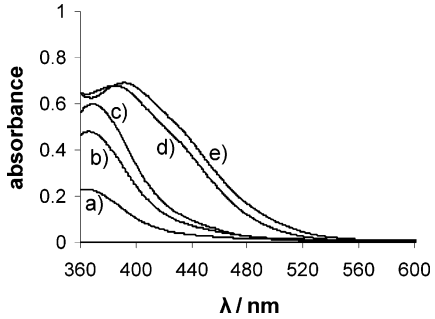

Figure 5. UV−vis absorption spectra of microemulsions containing BiOI particles. Curves (a)−(e) correspond to increasing $R_w = 2$, 4, 6, 8, and 10, respectively.

Depending on the R_w-value and the concentration of the salts in the aqueous phases, colors ranging from pale yellow to dark orange could be observed. Figure 4 shows a photograph of isolated BiOI nanoparticles with increasing particle size. The color change can be explained with the quantum-size effect for nanosized semiconductor materials. With decreasing particle size, the band gap energy increases. The quantum-size effect in BiOI nanoparticles can be directly seen in color changes of the microemulsions with variable R_w-value. This observation could be confirmed by UV−vis spectroscopy. Figure 5 shows UV−vis spectra of microemulsions containing BiOI nanoparticles with increasing R_w-value. With decreasing R_w-value, the absorption edge is shifted to shorter wavelengths, corresponding well with the expectations derived from quantum-size theory. For BiOI microemulsions with $R_w = 2$, showing a pale yellow color, the onset was determined at 419 nm. The shift to higher wavelengths for higher R_w is only small for $R_w = 4$ (424 nm) and $R_w = 6$ (429 nm). A clear shift can be observed moving from $R_w = 6$ to $R_w = 8$. The onset was determined at 492 nm ($R_w = 8$) and 496 nm for $R_w = 10$. The decreasing absorption for smaller R_w-values is caused by decreasing BiOI concentrations.

Not only the composition of the microemulsions and resulting micelle sizes had an influence on particle growth. With constant R_w-value and micelle size, the particle size could be influenced by the ratio of the involved salt solutions in the aqueous phases of microemulsions. The ratio BiO^+/I^- was varied from 0.5:1 to 1:0.5 at constant $R_w = 8$. UV−vis spectra (Figure 6) show a significant shift of the absorption band to shorter wavelengths for an excess of BiO^+ (Figure 6a). For a BiO^+/I^--ratio of 1:0.5, the onset could be found at 477 nm, compared to 492 nm at a 1:1 ratio and 536 nm for an excess of I^-. The lower absorption for the samples with nonstoichiometric concentrations is again due to lower BiOI concentration in the microemulsions.

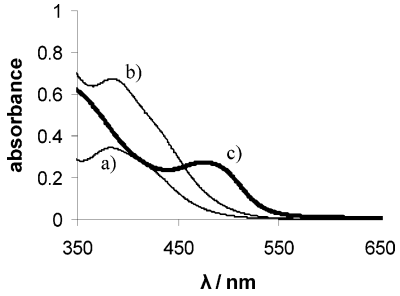

Figure 6. UV−vis absorption spectra of microemulsions (R_w = 8) containing BiOI: (a) BiO^+/I^- = 1:0.5; (b) BiO^+/I^- = 1:1; and (c) BiO^+/I^- = 0.5:1.

(c) X-ray Diffraction (XRD) Analysis. BiOX nanoparticles were isolated from their microemulsions by centrifugation. For some R_w-values and concentrations, the particles could be isolated directly. Particles in stable microemulsions not agglomerating after 24 h of stirring could be isolated by evaporating the solvent from the microemulsions until the particles precipitated. Excess surfactant could be removed only partially from the obtained substance by washing several times with heptane and ethanol. X-ray powder diffraction patterns were recorded from the as-dried powders. The crystallinity was high enough, and subsequent thermal treatments were not necessary. The observed powder patterns are in good agreement with those reported in the literature for BiOCl, BiOBr, and BiOI[51] but with broad peaks due to size broadening.

Parts a−c of Figure 7 show X-ray powder diffraction patterns for BiOCl, BiOBr, and BiOI with increasing R_w at BiO^+/I^--ratios = 0.5:1. Patterns for all particles BiOCl, BiOBr, and BiOI showed some degree of anisotropic peak broadening. The effect was gaining importance with increasing particle size resulting from increasing R_w and the excess of counterions. For the calculation of the volume-weighted crystallite size using the Scherrer equation, the single peak widths were calculated. Peaks indexed as (*hkl*) with $l \neq 0$ such as (102), (212), (101), or (211) gave very small values for the crystallite sizes; in some cases, calculation of the peak widths was impossible, because single peaks were not resolved properly. In parts d−f of Figure 7, values calculated from peak (200) of BiOCl, and from peaks (110) and (200) of BiOBr and BiOI, are shown. For both peaks, l was zero (l = 0); thus, their broadening was associated with the particle extension in [100]- and [010]-direction without any

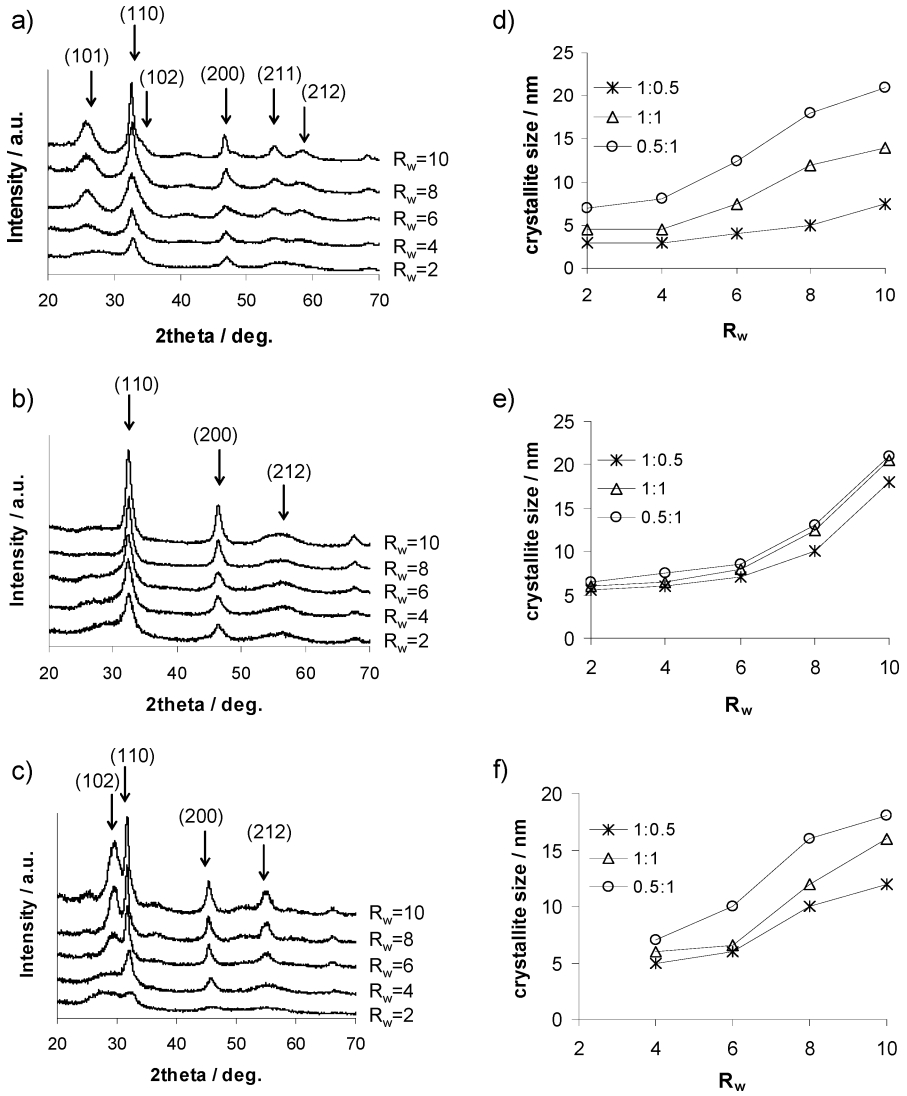

Figure 7. X-ray diffraction patterns of (a) BiOCl, (b) BiOBr, and (c) BiOI with BiO^+/Cl^- = 0.5:1 and increasing R_w = 2−10. Calculated crystallite sizes with increasing R_w and varying salt concentrations for (d) BiOCl, (e) BiOBr, and (f) BiOI.

component in [001]-direction. They were narrower and more distinctive than peaks with a component in the [001]-direction. These observations indicated that BiOX nanoparticles synthesized in the microemulsions are anisotropic in shape. From the X-ray diffraction patterns, we expect anisotropic nanoparticles with elongated edges parallel to [100] and/or [010]. Another possible source of anisotropic peak broadening is the formation of defects in the crystals.

As already mentioned above, for particle size calculations from X-ray powder patterns, the Scherrer equation was used, giving the volume-weighted thickness of the crystallite from the integral breadth of a reflection. In parts d−f of Figure 7, the calculated apparent crystallite sizes derived from peaks (110) and/or (200) for all samples are plotted vs R_w of the corresponding microemulsion used in the synthesis.

As expected, the micelle size had a strong influence on the size of the resulting crystallites. For all materials, the crystallite size was increasing with increasing R_w, but the relation was not linear. It is noteworthy that agglomeration did not affect the crystallite size. In all cases, the reverse micelles restricted the reaction volumes, resulting in nanosized crystallites.

For BiOCl particles, the increase with R_w was more or less constant. Remarkable differences could be observed for varying salt concentrations at constant R_w. These differences were even more distinctive for high R_w-values. At $R_w = 10$, the particle size calculated from XRD data was 7.5 nm for excess of BiO^+ (1:0.5) and 21 nm for excess of Cl^- (0.5:1). For BiOBr particles, the crystallite size increased just slightly at small R_w-values, and differences for concentration effects were negligible. Particularly for BiO^+/I^-- ratios 1:1 and 0.5:1, the obtained crystallite sizes were almost identical. A decreasing slope could be observed between $R_w = 6$ and $R_w = 10$. Within this region, the crystallite size increased from 8 nm for excess of BiO^+, and from 8.5 nm for excess of Br^-, to 20.5 nm or 21 nm, respectively. BiOI particles synthesized in a microemulsion with $R_w = 2$ showed very broad signals in X-ray diffraction patterns. Thus, the crystallite size was only calculated for particles resulting from microemulsions with $R_w = 4-10$. A similar trend as for BiOBr could be observed for BiOI nanoparticles. The increase in crystallite size was small for R_w values between 4 and 6. A remarkable increase can be found between $R_w = 6$ and $R_w = 10$, when the crystallite size increased from 6 nm ($R_w = 6$) to 10 nm ($R_w = 10$) for excess of BiO^+, and from 10 nm ($R_w = 6$) to 18 nm ($R_w = 10$) for excess of I^-. This observation is in good agreement with results from UV−vis spectra, with the shift of the absorption edge being, in particular, more pronounced going from 6 to 10 in R_w.

(d) Transmission Electron Microscopy (TEM). Parts a and b of Figure 8 show TEM images of BiOI particles isolated from a transparent microemulsion with $R_w = 8$ and with BiO^+/I^--ratio = 1:1 (sample BiOI-4, Table 3). The average diameter is 5−10 nm. Lattice fringes can be observed in high-resolution TEM images. The *d*-spacing in Figure 8b was determined as 3.78 and 2.27 Å, corresponding to the (101) and (004) *d*-spacing of BiOI (3.651 and 2.287 Å[51]).

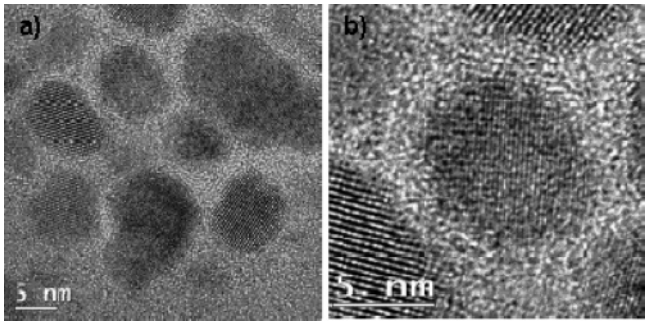

Figure 8. TEM images of BiOI nanoparticles from transparent microemulsion: (a) survey of nanoparticles 5−10 nm in size and (b) high-resolution electron mirograph showing lattice fringes.

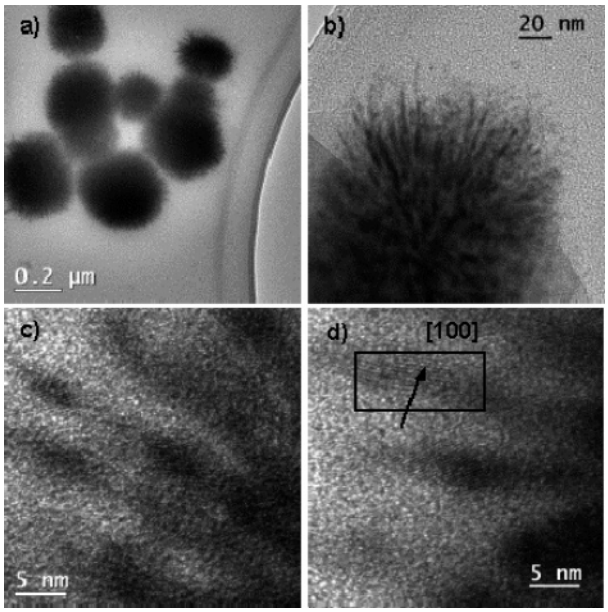

Figure 9. TEM images of BiOI nanoparticles after aging: (a)−(b) aggregates with concentrically ordered needles and (c)−(d) high-resolution electron micrographs showing (100) planes parallel to the long axis of the nanoneedles.

In order to explain the anisotropy observed in XRD patterns, samples for TEM analysis were prepared under similar conditions as for XRD analysis. Thus, the particle-containing microemulsion was allowed to age several days until becoming turbid due to agglomeration of the particles. The composition of the microemulsion was the same as above (sample BiOI-4, Table 3).

In parts a and b of Figure 9, dendritic aggregates can be observed, consisting of several concentric ordered nanoneedles. The size of the aggregates is 200−300 nm. Parts c and d of Figure 9 show single nanoneedles at higher magnification. The single crystals show a rodlike morphology with high aspect ratios. The length of the nanorods is not uniform and ranges from 10 to 20 nm. The diameter of the rods is 3−4 nm. These observations are in agreement with the anisotropic peak broadening observed in X-ray diffraction powder patterns. The crystallite size calculated from the (110) and (200) peaks is 12 nm; size broadening was more severe for reflections with $l \neq 0$. Lattice fringes can be observed in high-resolution TEM images. The *d*-spacing in Figure 9d was determined as 3.89 Å and is close to the size of the

(51) Sillen, L. G. *Svensk Kem. Tidskr.* **1941**, *53*, 39.

lattice parameter **a** (3.994 Å[51]). The growth axis is not identical for all needles.

Conclusion

An efficient synthesis for BiOCl, BiOBr, and BiOI nanoparticles was reported using reverse microemulsions. With the R_w-value and the concentrations of the involved salt solutions in the aqueous phases, the particle size was adjusted in between 3 and 22 nm. Using liquid- and solid-state characterization methods, we could provide a consistent picture about size and polydispersity of the synthesized nanoparticles. Controlling the particle dimensions allows adjusting the band gap, absorption edge, and color of BiOI nanoparticles due to the quantum-size effect. For BiOI, a shift of the band gap from 1.94 eV (carmine red) for the bulk material up to 2.96 eV (pale yellow) for BiOI nanoparticles was observed. Providing a broad color spectrum adjusted with the synthesis parameters, BiOI nanoparticles are promising components for color filters in transparent nanocomposite materials.

Acknowledgment. Generous support of the Federal Ministry of Education and Research (BMBF: FK 03X5502) is gratefully acknowledged. Surfactants were supplied by SASOL. We would like to thank Prof. H. Lichte and Dr. M. Lehmann for their support of TEM investigations at the Triebenberg Laboratory.

Supporting Information Available: The DLS results for the samples BiOCl-2, BiOCl-7, BiOCl-8, BiOBr-6, BiOI-4, BiOI-5, BiOI-10, BiOI-13, and BiOI-14, X-ray powder diffraction patterns of the samples BiOX 1-10, and an atomic force microscopy (AFM) image of spin-coated nanoparticles (BiOI-4) are available in the Supporting Information. This material is available free of charge via the Internet at http://pubs.acs.org.

CM061671K